



Department of Electrical and Computer Engineering
Senior Capstone Project
Active Suspension System

Students: Caleb Dell, Leslie Garcia, Alex Jaeger

Advisors: Prof. S. D. Gutschlag and Prof. Jing Wang

May 13th, 2019

Abstract

This paper describes the implementation of an active suspension system using various control methodologies. The basic active suspension system was constructed in 1990 and modified in 2006 to replace the pneumatic cylinder with a linear actuator as the mechanical position control device. Disturbance inputs were generated on the bottom plate by a camshaft driven by a three phase AC induction motor controlled by a variable-frequency drive (VFD). The electronically controlled linear actuator connected to the upper and lower plates limited the vertical motion of the upper plate so that its position was virtually constant independent of the disturbance input. The linear actuator shaft position was controlled by an Atmel Atmega128A microcontroller via digital control signals applied to an optically-coupled H-bridge that applied appropriate voltages to the linear actuator to extend or retract its output shaft as necessary to maintain the desired position. The initial control algorithm was a simple bang-bang controller intended merely to ensure the system control software and hardware functioned properly. This document also discusses the implementation of a proportional controller, and the research completed relative to the implementation of more complex Proportional-Integral (PI) and Proportional-Integral-Derivative (PID) digital control algorithms.

Table of Contents

I. Introduction	4
II. Subsystem Functional Requirements	4
III. Subsystem Functional Descriptions	5
A. Hardware	5
1. Upper and Lower Platform	5
2. Potentiometer	5
3. Safety Relays	5
4. Limit Switches	6
5. Linear Actuator	6
6. Rotating Camshaft	6
7. Basic System Electrical Hardware	6
8. Discrete Component H-bridge Test Circuit	6
B. Modeling and Control	7
1. Atmega128A Microcontroller Board:	7
2. Control System	7
IV. Work Completed	8
A. Schematic Diagram	8
B. Three-Phase Motor	8
C. H-Bridge	8
D. Bang-Bang Controller	9
E. Finding Coulomb Friction and Viscous Damping	14
F. Armature Inductance and Resistance	18
G. Gold standard	19
H. Simplifying Model	20
I. Proportional Controller	21
J. Keypad and LCD:	24
K. Frequency Responses	25
VII. Appendices	29
Appendix 1: Simulink Models	29
Appendix 2: MATLAB Code	29
Appendix 3: Embedded C Code	29
Appendix 4: Spreadsheets	29
Appendix 5: Part List	30
Appendix 6: Schematic of the Apparatus	31
VIII. References	32

I. Introduction

The primary goal of the Active Suspension System Senior Design Team (ASSSDT) was to design an active system capable of eliminating most of the vertical motion imparted to the supported platform by a disturbance input. The system is represented by the high-level block diagram shown in Figure 4-1. The ultimate use for such a system is most commonly to reduce the effect of disturbances imparted to a moving vehicle by rough terrain to provide a gentle ride for passengers. For this single actuator response arrangement, the lower platform of the system provides an oscillating vertical motion and the linear actuator attached to the lower platform will extend or retract as necessary to ensure the upper platform maintains the desired position specified by the user. The linear actuator was controlled by an optically-coupled H-bridge module connected to an Atmel Atmega128A microcontroller which permits the control algorithms to be coded using Embedded C.

II. Subsystem Functional Requirements

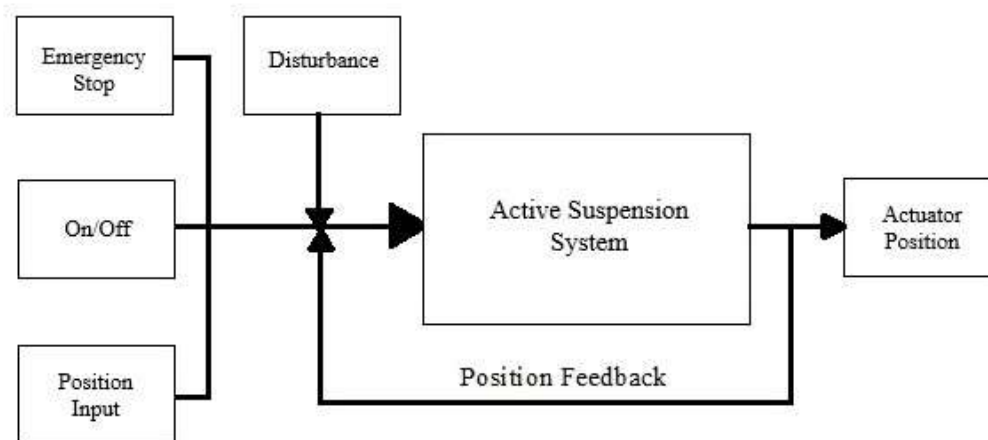


Figure 4-1: System Flow Diagram

The system is represented by the high-level block diagram shown in Figure 4-1. As indicated in Figure 4-1, the system incorporates three user inputs; the Emergency Stop, the ON/OFF switch, and a keypad and LCD panel to permit the user to enter the desired vertical position. The disturbance input is applied to the system, and the instantaneous position is fed back to the controller input to permit minimizing changes in the actuator position about the desired position set by the operator.

III. Subsystem Functional Descriptions

A. Hardware

1. Upper and Lower Platform

The system controller implemented with the Atmega128A microcontroller ensured that the upper platform's vertical motion was maintained at (or near) the desired position specified by the user. The lower platform oscillates in the vertical direction and was controlled by a three-phase AC induction motor connected to a camshaft as shown in Figure 5-1. The lower platform oscillation frequency was controlled by the three-phase AC variable-frequency drive (VFD) used to control the speed of the AC induction motor connected to the camshaft underneath the lower platform. It should be noted, however, that the camshaft under the lower platform does not provide true sinusoidal vertical motion because the VFD used to control the camshaft speed operates in a "constant torque" mode and not in a "constant speed" mode. Therefore, since the AC induction motor will not drive the camshaft at a constant rotational velocity, the lower platform's vertical motion approximated sinusoidal motion, but was in fact be slightly distorted.

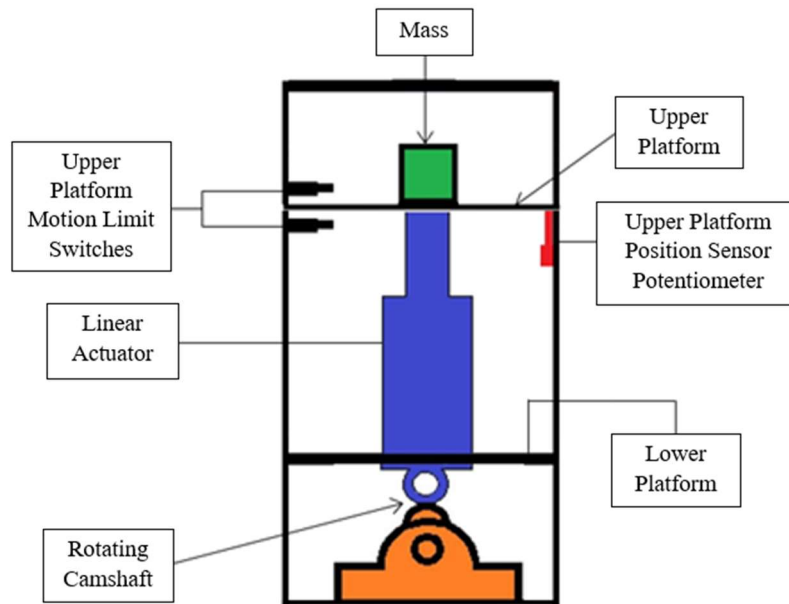


Figure 5-1: Active Suspension System

2. Potentiometer

There is one potentiometer vertically-mounted onto the system. The potentiometer is connected to the upper platform, as shown in Figure 5-1. The potentiometer was used to measure the instantaneous position of the respective platforms. When a control algorithm was applied to the active system, the lower platform moved a much larger distance than the upper potentiometer during normal operation.

3. Safety Relays

There were two OMRON MY4N-D2-DC24 4 pole relays utilized to provide for emergency system shut-down as shown in Figure 6-1. In the default position, the connection from the Maxi-Torq 4z394 AC induction motor is open, so the cam shaft will not rotate. Once a 24-volt DC signal is applied to pins 13 and 14 in both relays, the relay coils are active and the switches will close, disabling the brake (which is active low) and connecting the 3-phase source to the AC motor. Two components can switch the relay to its default position once in active mode: the two limit switches and the emergency stop button.

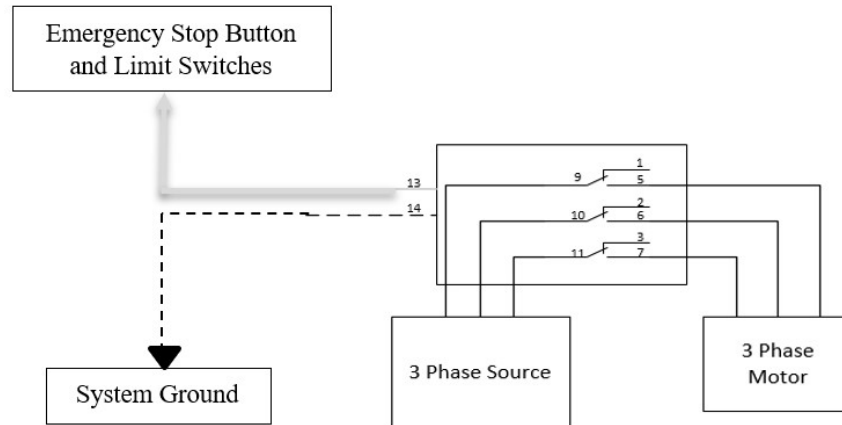


Figure 6-1: Three-Phase Motor Safety Relay in the Inactive (Normally-closed) Position

4. Limit Switches

There are two limit switches connected to the system, as shown in Figure 5-1. The switches were included in the system design to guarantee an upper and lower bound of motion in the event of a controller malfunction during development or due to a component failure after the system design was complete. When one of the limit switches is activated, both safety relays will switch to their normally open positions and all system motors will stop (except cooling fans). Note that the linear actuator has an internal brake that will also be activated to lock it in place. However, the AC induction motor is not equipped with a brake, so it will simply settle to its lowest position once it is turned off.

5. Linear Actuator

The linear actuator was driven by an optically-coupled H-bridge module connected to an Atmega128A microcontroller used to apply the control algorithms. The actuator is mounted to both the upper and lower platform as shown in Figure 5-1. The actuator will extend and retract to compensate for the lower platform movements based on the output of the potentiometer used as the upper position sensor. If the system is operating properly, the upper platform will maintain the position specified by the user input while the rotating camshaft continues to provide disturbances to the lower platform.

6. Rotating Camshaft

The rotating camshaft will rotate at all times during system operation unless the operator turns off the VFD to the three-phase AC induction motor or the emergency stop is activated. The camshaft is located at the bottom of the system, as shown in Figure 5-1. The lower platform oscillations are generated by the rotating camshaft driven by the AC induction motor and will simulate the rough terrain alluded to in the introduction.

7. Basic System Electrical Hardware

The white control box mounted to the top of the active suspension system contains the connections to all subsystems on the apparatus. This includes two LM317 voltage regulators set to provide 12[V] for the cooling fan, and a 3.3[V] source if needed for future modifications. One LM7815 voltage regulator was used to provide 15[V] which will act as VCC for the MSK H-bridge, and one LM7805 voltage regulator was used to provide 5[V] to the 6N137 optical isolators. There are two OMRON MY2N-D2 safety relays connected to the emergency stop button which can be used to deactivate the linear actuator motor and the AC induction motor driving the camshaft in an emergency. An optically-coupled MSK 4227 H-bridge connected to an Atmega128A microcontroller is used to control the direction and speed of the linear actuator motor as required to maintain the desired upper platform position.

8. Discrete Component H-bridge Test Circuit

An additional H-Bridge was constructed with discrete components for initial software testing to ensure the basic Atmega128A microcontroller software was reliable and fully functional before it was connected to the optically-coupled MSK4227 H-bridge on the actual active suspension system apparatus. The test circuit was considered

imperative because the team had only one of the MSK4227 H-bridges on hand, and a replacement is very expensive. However, in the event a replacement H-bridge was needed later during project development, two PS21A79 three-phase integrated circuit inverters purchased by the 2016-17 active suspension design team were available.

The additional H-bridge used for code testing utilized four STP22NS25Z N-channel MOSFETs and four Avago HCPL-3120 optocouplers. The process of designing and troubleshooting the additional H-bridge was also a very valuable experience because it helped the team better understand the operation of the H-bridge and the software required to effectively control DC motors connected to the system. This is especially true since the MSK 4227 H-bridge on the actual active suspension system apparatus uses bootstrap capacitor high-side drivers which are somewhat difficult to use in practice unless their operational details are thoroughly understood.

B. Modeling and Control

1. Atmega128A Microcontroller Board:

The Atmega128A Microcontroller was used to control the MSK4227 H-Bridge, which in turn controlled the direction and speed of the Industrial Devices Corporation EC2H-1016B-150-MP3-FT1E-BM24-L linear actuator on the apparatus. Various controller algorithms were implemented with the Atmega128A microcontroller board to control the upper platform motion. The bang-bang controller was the most simplistic to implement in software, so it was used as the initial control algorithm to ensure the basic apparatus feedback system components were functional. The high-level software flow diagram for the bang-bang controller algorithm is shown in Figure 7-1 below.

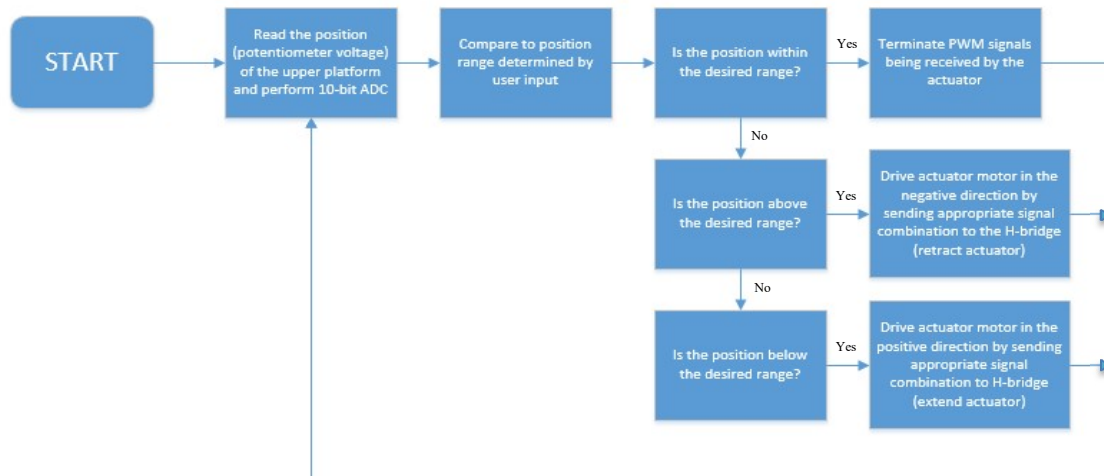


Figure 7-1: Bang-Bang Controller Software Flow Diagram

2. Control System

An s-domain model of the linear actuator was developed in Simulink to simulate operation under various load conditions and input voltages. All of the various control system algorithms used an Atmega128A PWM motor control signal and the position detected by the upper platform sensor as the feedback control signal. A bang-bang controller algorithm was implemented initially to verify basic system functionality. Once functional, the team attempted to design a proportional digital feedback control algorithm to more effectively control the position of the upper platform.

IV. Work Completed

A. Schematic Diagram

Before testing the apparatus, it was already known from the 2016-17 active suspension design team's report that the three-phase AC motor was not functional. To diagnose the problem, the team reviewed the previous team's schematic diagram and realized a more comprehensive schematic diagram was needed before it would be possible to locate the problem. The updated schematic diagram is shown in Appendix 6. As discussed in the following section, the updated schematic diagram was used to verify connections and gain a more complete understanding of the modifications made to the system by the previous team.

B. Three-Phase Motor

After the system schematic diagram shown in Appendix 6 was completed, the team thoroughly tested the functionality of the active suspension apparatus electrical system. To locate the reason for the failure of the AC motor to operate, the team started troubleshooting the apparatus by first testing the emergency stop switch before applying the three-phase 208 [V] supply to the VFD used to control the three-phase AC motor speed. A 24 [V] DC power supply was connected to the circuit box to test the emergency stop switch for proper operation. As indicated in the system schematic diagram shown in the Appendix, the emergency stop switch will shut down the entire apparatus and activate the linear actuator brake if the switch is in the closed (depressed) position.

With the three-phase 208 [V] supply completely disconnected from the VFD (i.e., open-circuited), the team used an ohmmeter to test the connection from the relay VFD source inputs (pins 9, 10, and 11) to the 3-phase AC motor outputs (pins 1, 2, and 3) as installed by the previous team. The team discovered that with the 24 [V] DC power supply connected to the circuit box and the emergency stop switch in its deactivated position (i.e., not depressed), continuity was not present between the relay source pins from the VFD and the output pins connected to the 3-phase AC motor. However, when the emergency stop switch was subsequently activated (i.e., depressed), continuity was established. That result indicated the 3-phase AC motor was connected to the normally-closed relay output terminals instead of the normally-open terminals as required for proper operation. After switching the 3-phase AC motor relay connections to the normally-open terminals (pins 5, 6, and 7) as shown in Figure 6-1, the 3-phase AC motor functioned properly.

C. H-Bridge

Since only one MSK 4227 H-bridge was available, the design team decided to construct an H-bridge with bootstrap capacitor high-side drivers to gain a better understanding of the basic functionality and to test microcontroller code before the inputs were applied to the MSK 4227 H-bridge on the active suspension apparatus. As shown in Figure 9-1, the discrete component H-bridge consisted of 100[uF] bootstrap capacitors, IN4004PSP diodes, P22NS25Z N-channel MOSFETs, and Avago HCPL-3120 optocouplers. After doing some additional research and documenting Professor Gutschlag's explanation of the H-bridge functionality, the team was able to grasp the fundamentals of the bootstrap capacitor operation relative to the discrete component H-bridge. The discrete component H-bridge designed by the team used a test load consisting of a Pittmann DC motor connected between the upper and lower MOSFETs on both sides of the H-bridge.

The basic operation of the H-bridge can be described as follows. If inputs HINB and LINA are turned off, and input HINA is driven with a variable duty cycle Pulse-Width-Modulated (PWM) control signal with input LINB constantly turned on, the left side of the motor will be connected to the power supply and the right-hand side will be connected to ground. For this condition, Pulse-Width-Modulated current will flow through the motor such that it will rotate in the forward direction. Conversely, if inputs HINA and LINB are turned off, and input HINB is driven with a variable duty cycle Pulse-Width-Modulated control signal with input LINA constantly turned on, the right side of the motor will be connected to the power supply and the left-hand side will be connected to ground. For this condition, Pulse-Width-Modulated current will flow through the motor such that it

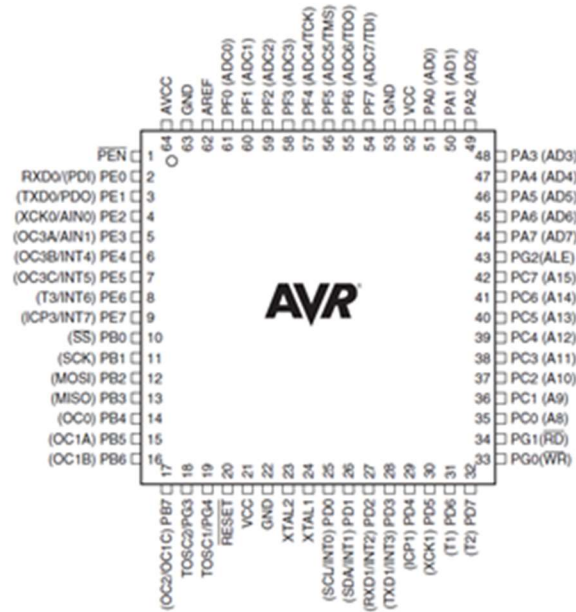


Figure 10-1: Atmel Atmega128A Microcontroller Pin-outs

The ports utilized for PWM generation were PB4 (designated by register OC0) and PB7 (designated by OC2) as shown in Figure 10-1. The pins PB4 and PB7 will be driving the HINA and HINB pins, respectively. Pin operation is initiated by configuring the TCCR0 and TCCR2 timer/counter control data registers represented in Figures 10-2 and 10-3.

Timer/Counter Control Register – TCCR0

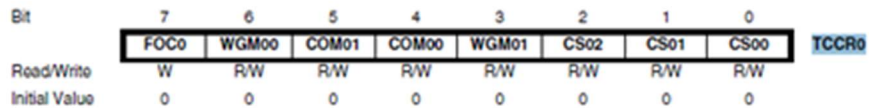


Figure 10-2: TCCR0 Data Register

Timer/Counter Control Register – TCCR2

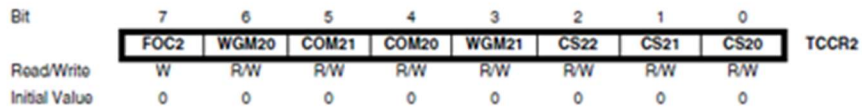


Figure 10-3: TCCR2 Data Register

Based on the Atmega128A microcontroller datasheet, FOC0 and FOC2 are zero in PWM mode. The WGM00 and WGM01 bits in TCCR0 determine the counting sequence of the counter. The team selected the “Fast PWM mode” for the counting method due to previous experience and ease of configuration. An arbitrary waveform timing diagram for Fast PWM mode operation is shown in Figure 11-1.

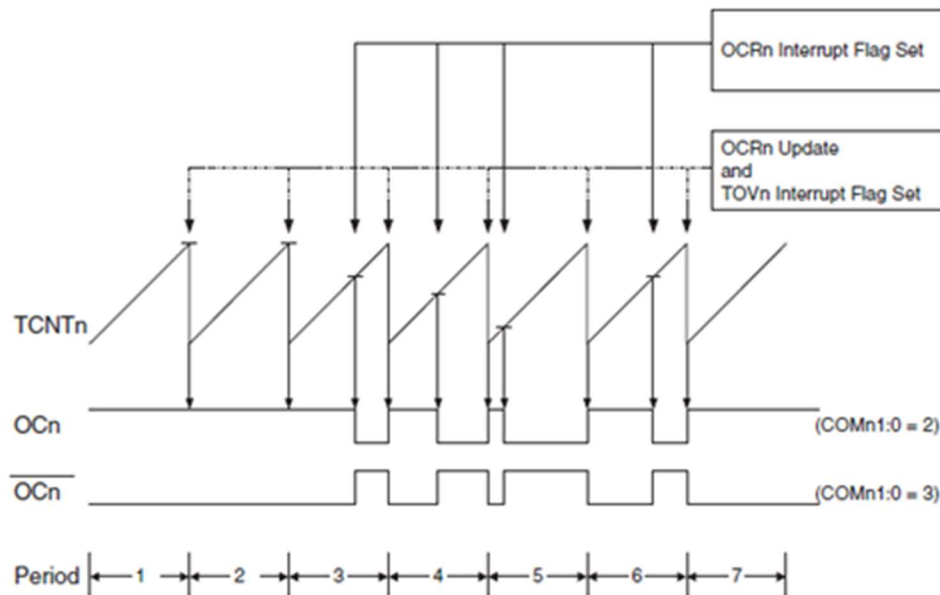


Figure 11-1: Atmega128A Fast PWM Mode Timing Diagram Example

The function of the OC0 output when operating in the Fast PWM mode depends on the configuration of the COM01 and COM00 register bits in timer/counter control data register, TCCR0. The team selected non-inverting mode which clears the OC0 output pin on a “compare register match” of TCNT0 and OCR0.

The CS02, CS01, and CS00 register bits determine the frequency of the PWM signal by selecting a prescaler that will divide the clock frequency by a fixed value to reduce the timer/counter operating frequency. The team selected a prescaler of 64 which corresponds to a timer/counter operating frequency of 976.56 [Hz] using the following equation obtained from the datasheet, where N is the prescaler value.

$$f_{OCnPWM} = \frac{f_{clk\ IO}}{N \cdot 256}$$

Eq. 11-1: PWM Signal Frequency Equation as a Function of the Selected Prescaler Value

The signal frequency was selected to obtain a reasonable compromise between minimizing motor noise and avoiding high-frequency switching losses. At lower switching frequencies, the linear actuator motor noise levels will be greater due to the significant vibrations associated with the motor armature (rotor) caused by the magnetostriction induced by the rapidly changing armature currents. Although switching at higher frequencies will reduce motor noise levels, it will result in higher average MOSFET power losses due to the increased number of switching cycles per second. Higher switching losses occur at higher switching frequencies because the low and high-side MOSFETs both conduct the same average current during the switching process. In addition, both MOSFETs also experience the same average voltage during the switching process. Therefore, as the switching frequency increases, so must the average power dissipation due to switching losses.

TCCR2 is set up the basically the same as TCCR0, but with a slight difference associated with the prescaler selection. TCCR2 allows for external clock sources when determining the frequency of the PWM signal, which limits the choice of prescaler for dividing the clock frequency. However, both timer/counters had the option to permit selecting a prescaler of 64 so both PWM outputs could be set to the desired frequency of 976.56 [Hz].

The duty cycle of the PWM signal was determined by setting the OCR0 data register. The maximum count for the TCNT0 and TCNT2 registers is 255 since they are both 8-bit counters. OCR0 will determine when the OC0 pin is cleared in the non-inverting mode. For example, a 50% duty cycle is achieved by setting OCR0 to 128 in the non-inverting Fast PWM mode of operation. The TCNT0 and OCR0 registers are shown in Figures 12-1 and 12-2, and the TCNT2 and OCR2 registers are shown in Figures 12-3 and 12-4.

Timer/Counter Register – TCNT0

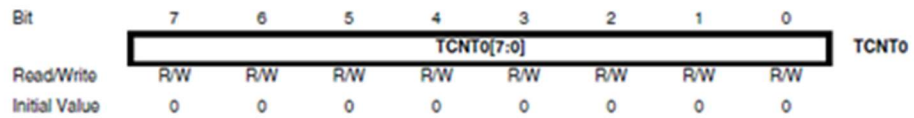


Figure 12-1: TCNT0 Data Register

Output Compare Register – OCR0

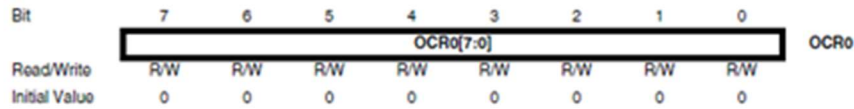


Figure 12-2: OCR0 Data Register

Timer/Counter Register – TCNT2

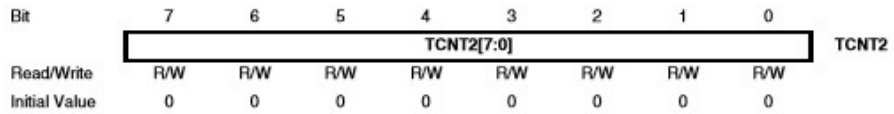


Figure 12-3: TCNT2 Data Register

Output Compare Register – OCR2

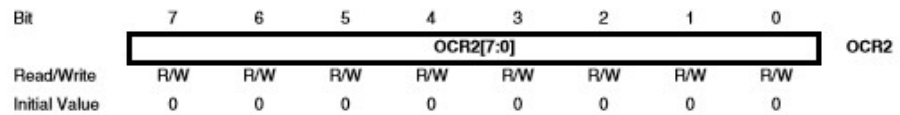


Figure 12-4: OCR2 Data Register

The same process is used for TCCR2 with the data registers TCNT2 and OCR2 referring to the timer and output compare register for the signal on OC2 respectively. With the PWM signals set up, the team developed software to switch between the two signals.

To control the LINA and LINB sections of the H-bridge, PORTE pins 0 and 1 (respectively) are used as simple I/O pins to be set high or low depending on desired operation.

On the apparatus, a linear potentiometer measures the position of the upper plate. An external 5[V] source acts as the supply for the potentiometer, although the 5[V] microcontroller source could be used as well. The stroke length of the actuator is 6 inches, which corresponds to the maximum 5[V] measurement with the potentiometer.

An ADC is required for the microcontroller to take the potentiometer reading as an input into the program. Pin PF0, designated as ADC0, will be used for the single channel ADC input. The ADC will convert the analog voltage from the potentiometer to a 10-bit number ranging from 0 to 1023. Initializing the ADC involves the registers ADCSRA and ADMUX shown in Figures 12-5 and 13-1.

ADC Multiplexer Selection Register – ADMUX

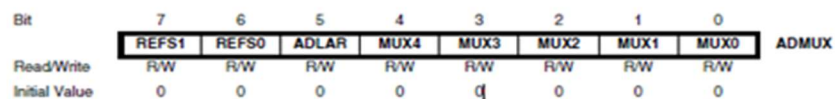


Figure 12-5: ADMUX Data Register

ADC Control and Status Register A – ADCSRA

Bit	7	6	5	4	3	2	1	0	
	ADEN	ADSC	ADFR	ADIF	ADIE	ADPS2	ADPS1	ADPS0	ADCSRA
Read/Write	R/W	R/W	R/W	R/W	R/W	R/W	R/W	R/W	
Initial Value	0	0	0	0	0	0	0	0	

Figure 13-1: ADCSRA Data Register

ADMUX is used to determine the reference voltage, the adjustment of the result, and the channel that the result is sent to. For the purpose of the 5[V] potentiometer, the internal reference is used. The left adjust option is not utilized, and since only one channel is necessary for the given application, ADC0 was selected with the ADMUX.

The ADCSRA register is manipulated when conversion takes place. Due to familiarity in previous applications using the ADC, the team used a prescaler of 16 to obtain a 1 MHz sampling frequency. To enable the ADC, ADEN is set to 1. To start a conversion, ADSC is set to 1, and the ADSC bit will read 0 when the conversion is complete. In the program “init_adc.c,” the team uses a while loop to remain in the loop when the ADSC bit is still high. Note that if desired, an ADC interrupt can be used.

As can be observed in the software flow diagram shown in Figure 7-1 for the bang-bang controller, the program will begin with an ADC operation to read the current position of the upper platform. This value will be compared to a user selected value between 0 and 1023. If the current position is less than the selected value, the program will disable TCCR2 and enable TCCR0 to output a PWM signal with a constant duty cycle on the OC0 pin to extend the linear actuator shaft. Since the MSK H-bridge has active low LINA and LINB channels, the corresponding pin on PORTE will be set to low with the other set to high. Conversely, if the current position is greater than the selected value, the program will disable TCCR0 and enable TCCR2 to output a PWM signal with a constant duty cycle on the OC2 pin to retract the linear actuator shaft.

```
int main(void)
{
    initialize();
    init_timers();
    init_adc();
    sei();

    while(1)
    {

        uint16_t adc_value=adc_read(); // get 10 bits
        if(adc_value>492 && adc_value<532)
        {
            TCCR0 = 0x00;
            TCCR2 = 0x00;
            PORTA = 0xff;
        }
        else if(adc_value>532)
        {
            PORTA = 0x00;
            TCCR2 = 0x00; //TCCR2=0b01101011;
            TCCR0 = 0b01101100; //TCCR2=0b01101011;
            OCR0 = 51;
            PORTC = 0b00000001;
        }
        else
        {
            PORTA = 0x00;
            TCCR0 = 0x00; //TCCR0=0b01101100;
            TCCR2 = 0b01101011;
            OCR2 = 51;
            PORTC = 0b00000010;
        }
    }
}
```

Figure 13-2: Main While Loop of Bang-Bang Controller

```

void init_adc(void)
{
    // A/D converter setup:
    // ADMUX - ADC Multiplexer Selection Register
    // AVCC with external capacitor at AREF pin, Bit 7:6 REFS1:0: 01
    // Bit 5 ADLAR: ADC Left Adjust Result, do not adjust, bit = 0
    // Mux selected for channel 0: Bits 4:0 00000
    ADMUX=0b01000000;
    // ADCSRA - ADC Control and Status Register A
    // Bits 2:0 ADPS2:0: ADC Prescaler Select Bits: Divide by 16 for 1MHz sampling
    // Bits 2:0 100
    // Bit 7 ADEN: ADC Enable = "1"
    // Bit 6 ADSC: ADC Start Conversion= "1"
    // Bit 5 ADFR: Free running = "0"
    // Bit 4 ADIF: Interrupt Flag ="0"
    // Bit 3 ADIE: Interrupt Enable = "0"
    ADCSRA=0b11000100;
    while(ADCSRA & 0x40);
    // start conversion since first one takes longer
    // Wait for conversion to complete, ADSC=Bit6 =0?
}
    
```

Figure 14-1: ADC Initialization

F. Finding Coulomb Friction and Viscous Damping

In preparation for the design of a Proportional controller, a Simulink model was created to conduct research prior to implementing modifications to the active suspension apparatus. A previous design team had created a Simulink model for the system, but there were several numerical values critical for a comprehensive model missing. Although some useful information was found in the linear actuator datasheets, the Coulombic (or kinetic) friction constant and the viscous damping coefficient were not available.

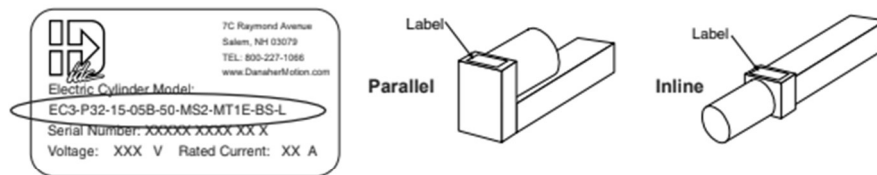
To obtain values of those critical variables, the datasheet for the linear actuator was used to obtain information that was used when the Coulombic friction constant and viscous damping coefficient were determined experimentally. From the model number obtained from the nameplate of the linear actuator within our apparatus, Figure 14-2 was used to find specific details for the equipment.

Cylinder Part Numbers - Identifying a Cylinder

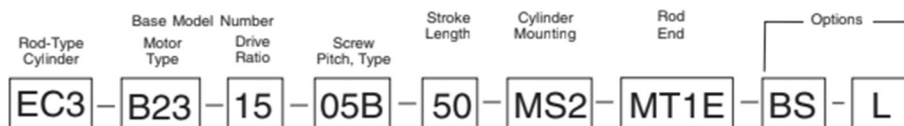
Your new EC cylinder will arrive with an IDC factory label attached as shown below. The factory label provides a detailed breakdown of the cylinder model with all of its mechanical characteristics. This section can be used to: 1) identify a cylinder's mechanical characteristics based on the factory label, or 2) order a new EC cylinder with different mechanical characteristics.

Label Location

Locations of Labels on Different Motor-Mounting Configurations



Model Number Example



- EC3** = Product Series
- B23** = NEMA 23 Frame, Brushless Servo Motor
- 15** = 1.5 to 1 Drive Ratio - Belt/Pulley
- 05B** = 5 mm Lead Ballscrew
- 50** = 50-inch stroke
- MS2** = Side Lugs Mounting
- MT1E** = Male Threaded Rod End - English Threads
- BS** = Brake on Screw Option
- L** = Linear Potentiometer Option

Figure 14-2: Linear Actuator Model Number Breakdown

Once all necessary datasheet information was documented, a variety of tests were conducted to compute the Coulombic friction constant, T_c , and the viscous damping coefficient, b . Although theoretically b would remain constant while T_c increases slightly with increases in load, the design team assumed both would be constants.

Tests were also run without the upper platform to see how the apparatus functions without any load. To compute T_c and b , the average linear actuator motor current (I_{ave}) and vertical shaft position (P_V) were measured with an oscilloscope. I_{ave} was found by attaching an oscilloscope current probe to the wire entering the positive terminal of the linear actuator motor. P_V was found by using an oscilloscope to record the voltage from the potentiometer built into the linear actuator on the apparatus. Two tests were conducted using a step input voltage of 40[V] with a period of 500[ms], but with two different duty cycles of 60% and 90%. Values for P_V and I_{ave} were experimentally obtained from single-sequence oscilloscope plots using display cursor measurements after applying the step inputs to the linear actuator.

Equation 15-1 was used to solve for the linear velocity associated with the linear actuator shaft.

$$\text{EQ. 15-1: } V \left[\frac{in}{sec} \right] = \frac{P_{V1} \cdot .6}{t}$$

$$V_1 \left[\frac{in}{sec} \right] = \frac{P_{V1} \cdot .6}{t} \rightarrow \frac{2 \cdot .6}{0.5} \rightarrow 4.8 \left[\frac{in}{sec} \right], \text{ where } P_{V1} = 2 \text{ [in]}$$

$$V_2 \left[\frac{in}{sec} \right] = \frac{P_{V2} \cdot .6}{t} \rightarrow \frac{3.3 \cdot .6}{0.5} \rightarrow 7.92 \left[\frac{in}{sec} \right], \text{ where } P_{V2} = 3.3 \text{ [in]}$$

Equation 15-2 was used to solve for the angular velocity using the linear actuator linear velocities found in Equation 15-1.

$$\text{EQ. 15-2: } \omega \left[\frac{rad}{sec} \right] = \frac{1 \text{ [rev]} \cdot 25.4 \text{ [mm]} \cdot 2\pi \text{ [rad]} \cdot V \text{ [in]}}{16 \text{ [mm]} \cdot 1 \text{ [in]} \cdot 1 \text{ [rev]} \cdot 1 \text{ [sec]}}$$

$$\omega_1 \left[\frac{rad}{sec} \right] = \frac{1 \text{ [rev]} \cdot 25.4 \text{ [mm]} \cdot 2\pi \text{ [rad]} \cdot V_1 \text{ [in]}}{16 \text{ [mm]} \cdot 1 \text{ [in]} \cdot 1 \text{ [rev]} \cdot 1 \text{ [sec]}} \rightarrow 47.85 \left[\frac{rad}{sec} \right]$$

$$\omega_2 \left[\frac{rad}{sec} \right] = \frac{1 \text{ [rev]} \cdot 25.4 \text{ [mm]} \cdot 2\pi \text{ [rad]} \cdot V_2 \text{ [in]}}{16 \text{ [mm]} \cdot 1 \text{ [in]} \cdot 1 \text{ [rev]} \cdot 1 \text{ [sec]}} \rightarrow 78.86 \left[\frac{rad}{sec} \right]$$

Equation 15-3 was used to solve for the torque constant in [(lb·in)/A].

$$\text{EQ. 15-3: } K_T \left[\frac{lb \cdot in}{A} \right] = \frac{54 \text{ [Oz in]} \cdot 1 \text{ [lb]}}{A \cdot 16 \text{ [Oz]}} \rightarrow 3.375 \left[\frac{lb \cdot in}{A} \right]$$

Equation 15-4 was used to solve for the average torque constants. Average current was found for both tests, where I_{Ave1} correlates to 60% duty cycle, while I_{Ave2} correlates to 90% duty cycle. Measurements indicated that $I_{Ave1} = 740 \text{ [mA]}$ and $I_{Ave2} = 815 \text{ [mA]}$.

$$\text{EQ. 15-4: } T_{Ave} \left[\frac{lb}{in} \right] = K_T \cdot I_{Ave}$$

$$T_{Ave1} \left[\frac{lb}{in} \right] = K_T \cdot I_{Ave1} \rightarrow 3.375 \cdot 0.74 \rightarrow T_{Ave1} = 2.498 \text{ [lb} \cdot \text{in]}$$

$$T_{Ave2} \left[\frac{lb}{in} \right] = K_T \cdot I_{Ave2} \rightarrow 3.375 \cdot 0.815 \rightarrow T_{Ave2} = 2.751 \text{ [lb} \cdot \text{in]}$$

With the information obtained from Equations 15-1 through 15-4, the average torque due to the sum of T_c and b can be expressed by Equation 15-5. Then Equation 16-1 can be used to develop equations to solve for T_c in Equation 16-2.

$$\text{EQ. 15-5: } T_{Ave} \left[\frac{lb}{in} \right] = T_c + (b \cdot \omega)$$

$$\text{EQ. 16-1: } T_C \left[\frac{lb}{in} \right] = \frac{(T_{Ave} \cdot \omega_1) - (T_{Ave1} \cdot \omega_2)}{\omega_1 - \omega_2}$$

$$T_C \left[\frac{lb}{in} \right] = \frac{(2.751)(47.85) - (2.498)(78.86)}{(47.85) - (78.86)} \rightarrow T_C = 2.1063 [lb \cdot in]$$

After T_c was computed, Equation 16-2 was used to solve for b for each data set. As expected, the computed value for b is identical for both experimental cases.

$$\text{EQ. 16-2: } T_C = T_{Ave1} - (b_1 \cdot \omega_1) \rightarrow 2.1063 [lb \cdot in] = 2.498 [lb \cdot in] - b_1 \cdot 47.85 \left[\frac{rad}{sec} \right]$$

$$b_1 = 0.00817525 \left[\frac{lb \cdot in}{rad/sec} \right]$$

$$T_C = T_{Ave2} - (b_2 \cdot \omega_2) \rightarrow 2.1063 [lb \cdot in] = 2.751 [lb \cdot in] - b_2 \cdot 78.86 \left[\frac{rad}{sec} \right]$$

$$b_2 = 0.00817555 \left[\frac{lb \cdot in}{rad/sec} \right]$$

To further verify the values of b and T_c , additional experimental trials were completed with the upper platform on the apparatus attached to the linear actuator shaft. For these experiments, the potentiometer connected to the upper plate was used to find position in terms of the potentiometer voltage, and again the average motor current was measured using an oscilloscope current probe. Table 16-1 shows the results of each experimental trial.

	Voltage [V]	Duty Cycle	Period [s]	Ave. Current [A]	Position [V]
Trial 1	40	60%	0.5	0.99	1.70
Trial 2	40	90%	0.5	1.13	3.02
Trial 3	50	90%	0.5	1.19	4.00
Trial 4	60	90%	0.3	1.36	2.83

Table 16-1: Experimental data with the Upper Platform Attached

The data contained in Table 16-1 was used to find linear velocity, rotational velocity, and average torque. As for the case without the upper platform attached to the linear actuator shaft, two trials were needed to find T_c and b using the same set of system of equations. As shown below, Equations 16-3 through 17-4 were used to compute the values for T_c and b used in the comprehensive Simulink linear actuator model.

$$\text{EQ. 16-3: } V [in/sec] = \frac{P_{V1} \cdot 6}{t}$$

$$V_1 \left[\frac{in}{sec} \right] = \frac{P_{V1} \cdot 6}{t} \rightarrow \frac{1.7}{0.5} \cdot 6 \rightarrow 4.08 \left[\frac{in}{sec} \right], \text{ where } P_{V1} = 1.70 [in]$$

$$V_2 \left[\frac{in}{sec} \right] = \frac{P_{V2} \cdot 6}{t} \rightarrow \frac{3.02}{0.5} \cdot 6 \rightarrow 7.25 \left[\frac{in}{sec} \right], \text{ where } P_{V2} = 3.02 [in]$$

$$V_3 \left[\frac{in}{sec} \right] = \frac{P_{V3} \cdot 6}{t} \rightarrow \frac{4}{0.5} \cdot 6 \rightarrow 9.6 \left[\frac{in}{sec} \right], \text{ where } P_{V3} = 4.00 [in]$$

$$V_4 \left[\frac{in}{sec} \right] = \frac{P_{V4} \cdot 6}{t} \rightarrow \frac{2.83 \cdot 6}{0.5} \rightarrow 11.32 \left[\frac{in}{sec} \right], \text{ where } P_{V4} = 2.83 [in]$$

EQ. 17-1:

$$\omega \left[\frac{rad}{sec} \right] = \frac{1 [rev]}{16 [mm]} \frac{25.4 [mm]}{1 [in]} \frac{2\pi [rad]}{1 [rev]} \frac{V[in]}{1 [sec]}$$

$$\omega_1 \left[\frac{rad}{sec} \right] = \frac{1 [rev]}{16 [mm]} \frac{25.4 [mm]}{1 [in]} \frac{2\pi [rad]}{1 [rev]} \frac{4.08 [in]}{1 [sec]} \rightarrow 40.70 \left[\frac{rad}{sec} \right]$$

$$\omega_2 \left[\frac{rad}{sec} \right] = \frac{1 [rev]}{16 [mm]} \frac{25.4 [mm]}{1 [in]} \frac{2\pi [rad]}{1 [rev]} \frac{7.25 [in]}{1 [sec]} \rightarrow 72.3 \left[\frac{rad}{sec} \right]$$

$$\omega_3 \left[\frac{rad}{sec} \right] = \frac{1 [rev]}{16 [mm]} \frac{25.4 [mm]}{1 [in]} \frac{2\pi [rad]}{1 [rev]} \frac{9.60 [in]}{1 [sec]} \rightarrow 95.80 \left[\frac{rad}{sec} \right]$$

$$\omega_4 \left[\frac{rad}{sec} \right] = \frac{1 [rev]}{16 [mm]} \frac{25.4 [mm]}{1 [in]} \frac{2\pi [rad]}{1 [rev]} \frac{11.32 [in]}{1 [sec]} \rightarrow 112.92 \left[\frac{rad}{sec} \right]$$

EQ. 17-2:

$$T_{Ave} \left[\frac{lb}{in} \right] = K_T \cdot I_{Ave}$$

$$T_{Ave1} \left[\frac{lb}{in} \right] = K_T \cdot I_{Ave1} \rightarrow 3.375 \cdot 0.99 \rightarrow T_{Ave1} = 3.34 [lb \cdot in]$$

$$T_{Ave2} \left[\frac{lb}{in} \right] = K_T \cdot I_{Ave2} \rightarrow 3.375 \cdot 1.13 \rightarrow T_{Ave2} = 3.81 [lb \cdot in]$$

$$T_{Ave3} \left[\frac{lb}{in} \right] = K_T \cdot I_{Ave3} \rightarrow 3.375 \cdot 1.19 \rightarrow T_{Ave2} = 4.02 [lb \cdot in]$$

$$T_{Ave4} \left[\frac{lb}{in} \right] = K_T \cdot I_{Ave4} \rightarrow 3.375 \cdot 1.36 \rightarrow T_{Ave2} = 4.59 [lb \cdot in]$$

Trials 1 and 3 were used for the computation of T_c and b because they exhibit the widest range in average current and linear velocity. Trial 2 had an average current and average velocity very similar to trial 3, and therefore did not exhibit a wide enough variation in values to provide accurate results. Also, the input voltage used for trial 4 was beyond the value expected to be applied to the apparatus during normal operating conditions for safety reasons, so that data was also not used for the computation of T_c and b .

EQ. 17-3:

$$T_C \left[\frac{lb}{in} \right] = \frac{(T_{Ave2} \cdot \omega_1) - (T_{Ave1} \cdot \omega_2)}{\omega_1 - \omega_2}$$

$$T_C \left[\frac{lb}{in} \right] = \frac{(4.02)(40.7) - (3.34)(95.8)}{(40.7) - (95.8)} \rightarrow T_C = 2.84 [lb \cdot in]$$

EQ. 17-4:

$$T_{C1} = T_{Ave1} - (b_1 \cdot \omega_1) \rightarrow 2.84 \left[\frac{lb}{in} \right] = 3.34 [lb \cdot in] - b_1 \cdot 40.7 \left[\frac{rad}{sec} \right]$$

$$b_1 = 0.012285 \left[\frac{lb \cdot in}{rad/sec} \right]$$

$$T_{C3} = T_{Ave3} - (b_3 \cdot \omega_3) \rightarrow 2.84 \left[\frac{lb}{in} \right] = 4.02 [lb \cdot in] - b_1 \cdot 95.8 \left[\frac{rad}{sec} \right]$$

$$b_3 = 0.012317 \left[\frac{lb \cdot in}{rad/sec} \right]$$

G. Armature Inductance and Resistance

The experimental procedure for verifying the armature resistance of the linear actuator motor involved applying various voltages across the armature power cable and measuring the current for each voltage applied. Using Ohm's Law, the resistance was calculated as shown in Table 18-1, with an average resistance of 7.83 $[\Omega]$.

Voltage [V]	Current [A]	Resistance $[\Omega]$
8.2	1.02	8.04
16.4	2.11	7.77
24.6	3.15	7.81

Table 18-1: Experimental Data to Verify Armature Resistance

Measuring the armature inductance of the actuator involved finding the time constant associated with the armature inductance and resistance. The time constant was found by measuring the armature current of the actuator motor after the source voltage was turned off as shown in Figure 18-1. The time constant is the amount of time it takes for the current to fall to 36.8% of its initial value. In Figure 18-1, the initial current is assumed to be the point in time when the response begins to display the distinctive shape expected of an exponentially decaying response. This was done for three different initial currents with the final inductance being computed as 40[mH].

Current [A]	Time [ms]	Inductance [mH]
1	5	39
2	5.2	41
3	6.24	46

Table 18-2: Experimental Data to Verify Armature Inductance

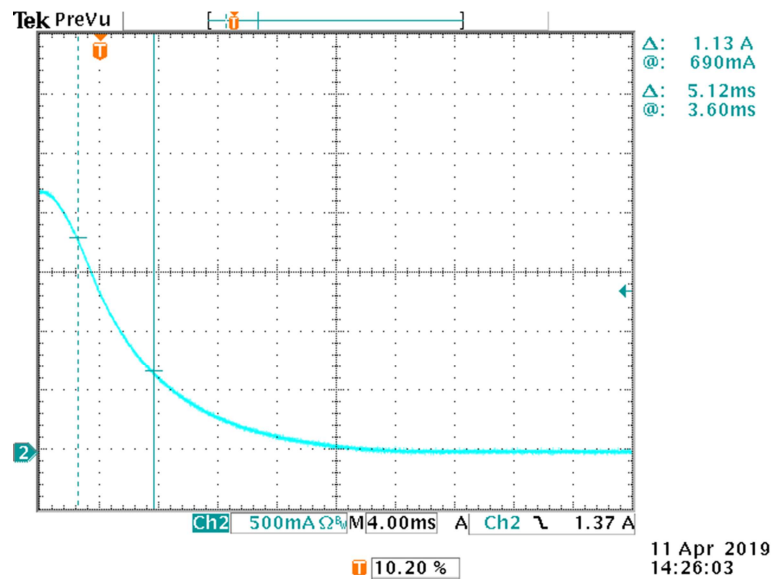


Figure 18-1: Current Response Used to Compute the Armature Inductance Time Constant

The time constant found with the initial current being 3[A] was ignored due to the nonlinearity of inductance due to leakage flux. Any current beyond the actuator's 2 [A] rating will force the ferromagnetic armature core into its saturated region, and therefore the computed inductance would correspond to the nonlinear region of operation. Obviously, if the model was to be for a linear system, this would be undesirable. Hence, the 40[mH] inductance obtained by using the average of the first two tests in Table 18-1 should be used as the value for the comprehensive Simulink model for the linear actuator system by all future teams simulating the apparatus.

H. Comprehensive Simulink Model for the Linear Actuator System

The actuator was modeled using Simulink (Appendix 1-C) for comparisons to the real system and the proportional controller. The values for the electrical and mechanical dynamics were calculated using information from the actuator data sheet.

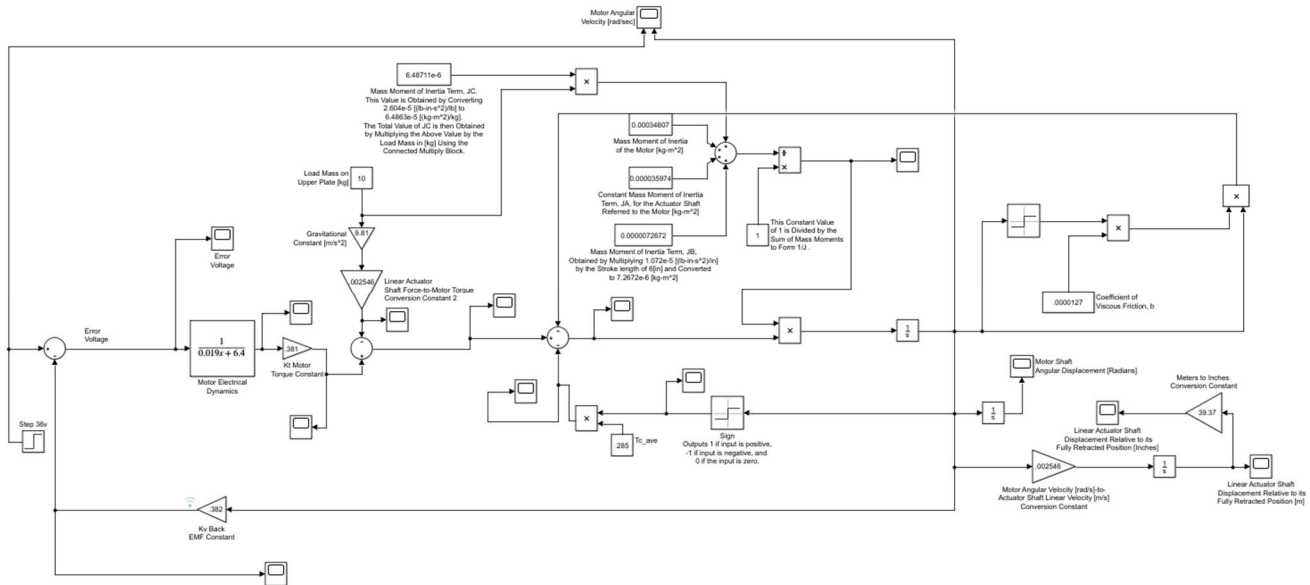


Figure 18-2: Gold Standard Simulink Model

The motor and actuator dynamics are modeled by the following blocks in Figure 18-2: “Motor Electrical Dynamics” and “Motor and Actuator Physical Dynamics.” The static load torque and the dynamic load torque are subtracted from the torque exiting the K_T constant block, yielding the torque available to accelerate the motor. The force to torque constant is calculated using Equation 19-1.

$$\text{Eq. 19-1:} \quad k = \frac{D}{2\pi} = 0.002546, \text{ where } D = \text{Screw Pitch} = 16 \text{ [mm]}$$

The mass moment of inertia of the motor is obtained by implementing Equation 19-2.

$$\text{Eq. 19-2:} \quad J_m = 3.063 \times 10^{-3} [\text{lb} \cdot \text{in} \cdot \text{s}^2] \times 0.0112985 \left[\frac{\text{Kg} \cdot \text{m}^2}{\text{lb} \cdot \text{in} \cdot \text{s}^2} \right] = 3.4607 \times 10^{-4} [\text{kg} \cdot \text{m}^2]$$

The constant mass moment of inertia term, J_A , for the actuator shaft referred to the motor is obtained by the Equation 19-3.

$$\text{Eq. 19-3:} \quad J_A = 3.184 \times 10^{-4} [\text{lb} \cdot \text{in} \cdot \text{s}^2] \times 0.0112985 \left[\frac{\text{Kg} \cdot \text{m}^2}{\text{lb} \cdot \text{in} \cdot \text{s}^2} \right] = 3.5974 \times 10^{-5} [\text{kg} \cdot \text{m}^2]$$

The mass moment of inertia term given the screw length of 6[inches], J_B , is obtained by using the Equation 19-4.

$$\text{Eq. 19-4:} \quad J_B = 1.072 \times 10^{-5} [\text{lb} \cdot \text{in} \cdot \text{s}^2] \times 6 \text{ [in]} \times 0.0112985 \left[\frac{\text{Kg} \cdot \text{m}^2}{\text{lb} \cdot \text{in} \cdot \text{s}^2} \right]$$

$$J_B = 7.2672 \times 10^{-4} [\text{kg} \cdot \text{m}^2]$$

The mass moments of inertia term associated with the load, J_c , is obtained by the Equation 19-5.

$$\text{Eq. 19-5:} \quad J_c = 2.604 \times 10^{-5} [\text{lb} \cdot \text{in} \cdot \text{s}^2] \times \text{Load [lb]} \times 0.249089 \left[\frac{\text{Kg} \cdot \text{m}^2}{\text{lb} \cdot \text{in} \cdot \text{s}^2} \right]$$

$$J_c = 6.4863 \times 10^{-5} [\text{kg} \cdot \text{m}^2]$$

The coulomb coefficient, T_c , and the viscous friction coefficient, b are obtained from Equation 17-4.

I. Simplifying the Model

To simplify the Simulink, model some decisions had to be made. The team decided to use ω instead of ω^2 since there is less than 5% of difference between the two models. The following, Figure 20-1 “Simplified Simulink Model”, is the theoretical block diagram for the active suspension system in which includes the electrical dynamic components and the mechanical dynamic components.

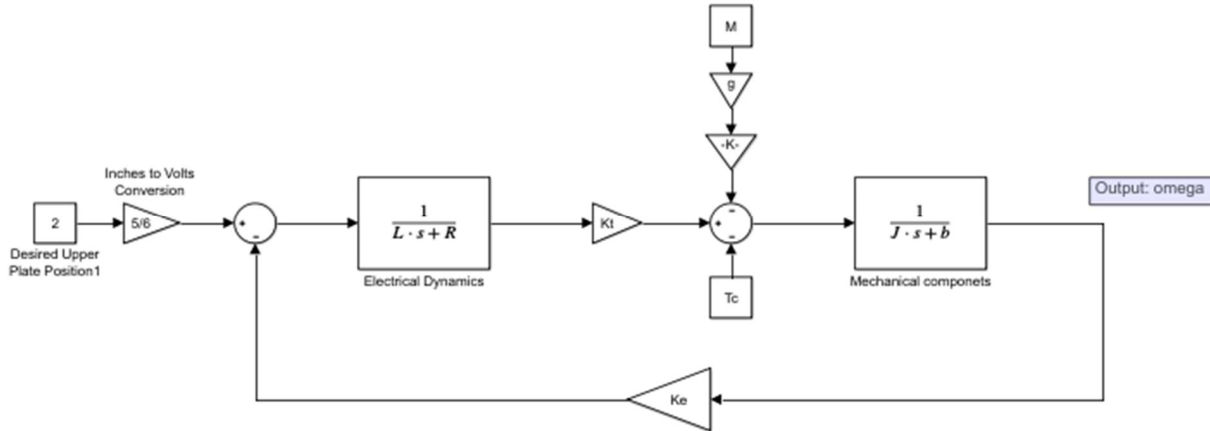


Figure 20-1: Simplified Simulink Model

where:

L: inductance (armature)

T_c : Coulombic friction

R: Resistance (armature)

J: Total moment of Inertia

K_t : Torque Constant

b: Viscous damping coefficient

M: Mass

K_e : Back EMF constant

g: Gravitational acceleration

K: Conversion constant

The decision was made to combine the J values for the purpose of simplifying the block diagram. To get the total J value, J_m , J_a , J_b , and J_c were added together, which is in Equation 20-1.

Eq. 20-1:
$$J_{Total} = J_M + J_A + J_B + J_C = 0.000418 \left[\frac{Kg \cdot m^2}{lb \cdot in \cdot s^2} \right]$$

Since the goal is to simplify the block diagram into one block, T_c , b , the load was removed, but they were compensated for in the new constants on Figure 20-2 “Block Diagram 2”.

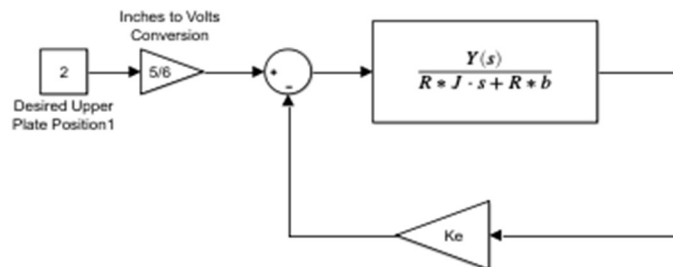


Figure 20-2: Block Diagram 2

Where $Y(s)$ is K_T for Figure 20-1 “Block Diagram 2” and for Figure 21-1 “Simplified Diagram”. Additional simplification leads to the simplified diagram shown in Figure 21-1.

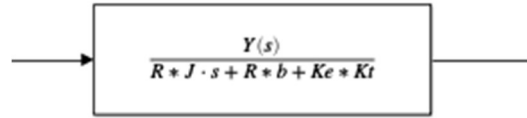


Figure 21-1: Simplified Diagram

The transfer function for Figure 21-1 is shown in Equation 21-2 below.

Eq. 21-2:
$$G(s) = \frac{Kt}{RJs + Rb + Kt \cdot Ke}$$

J. Proportional Controller

A proportional controller operates by scaling the error between the desired input and the current output of a system with a constant proportional gain. A proportional controller directly effects the step response of a system by reducing rise time as the proportional gain is increased, but also introduces a steady-state error that varies with the proportional gain. Higher values of proportional gain also tend to increase the settling time of the system, and can result in instability if the proportional gain is increased beyond a critical upper limit.

After fully simplifying the actuator model, position feedback and proportional gain were applied to the model. To design the optimal proportional gain, the controller and plant are combined to simulate the changes in the step response. Design considerations include rise time, settling time, and overshoot percentage. Figure 21-2 presents the appropriate equations to find the values for a generic 2nd order system.

$$K \frac{\omega_n^2}{s^2 + 2\zeta\omega_n s + \omega_n^2}$$

Generic 2nd order system

$\omega_d = \omega_n \sqrt{1 - \zeta^2}$ <p>Damped Natural Frequency Equation</p>	$T_r \cong \frac{\pi}{2\omega_n}$ <p>Rise Time Equation</p>
$M_p = e^{-\frac{\pi \zeta}{\sqrt{1 - \zeta^2}}}$ <p>Percent Overshoot Equation</p>	$T_s \cong \frac{4}{\zeta\omega_n}$ <p>Settling Time Equation</p>

Figure 21-2: Proportional Gain Design Equations

The design of the proportional gain began with a constant voltage model with the reduced actuator transfer function. In this model, the feedback is the upper platform position with units of potentiometer voltage (Vp) and the transfer function input will have units of voltage to drive the motor (Vd). A user-applied reference control voltage is compared to the current upper platform position feedback voltage to find the error (i.e., difference) between the two voltages. Note that the units for the user-supplied reference position and the Analog-to-Converter (ADC) feedback position will both be represented by a 10-bit binary value. Note also that the proportional gain will therefore have units of driving voltage per volt of error signal.

The next addition to the feedback control model converts the input signal applied to the actuator transfer function to a PWM voltage signal with a variable duty cycle and an amplitude of 40[V]. The 40[V] amplitude corresponds to the DC value of the source voltage applied to the apparatus in the laboratory during operation. The selected proportional gain is converted to percent duty cycle per volt of error signal shown in Figure 22-1.

After multiplying by 100, the output of the controller must be limited to a maximum of 93% duty cycle to provide adequate charge time for the bootstrap capacitors associated with the high-side power MOSFET drivers in the H-bridge.

The final controller model was programmed into the Atmega128A microcontroller. The microcontroller program converted the product of the error voltage and the proportional gain into a compare register value used by the microcontroller to form a duty cycle corresponding to the effective voltage required to adequately maintain the desired upper platform position. When the updated compare register value matches its associated timer/counter register, the PWM output is set to its low level for the remainder of the count cycle, thereby adjusting the duty cycle of the PWM H-bridge drive signal.

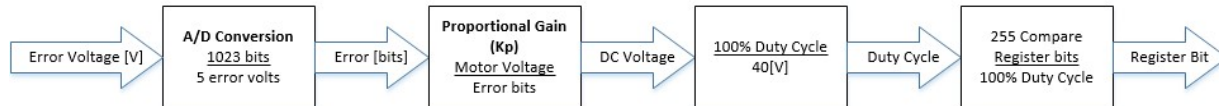


Figure 22-1: Proportional Gain Conversions

Figure 22-2 shows the high-level software flow diagram for the proportional controller program, which interfaces with the system in the same way as the bang-bang controller implemented in hardware first. Various selected gains were applied to the complete model used for simulation and the physical system for comparison. Figures 23-1 to 23-3 represent the simulated and experimental step responses of the proportional controller for three different gains.

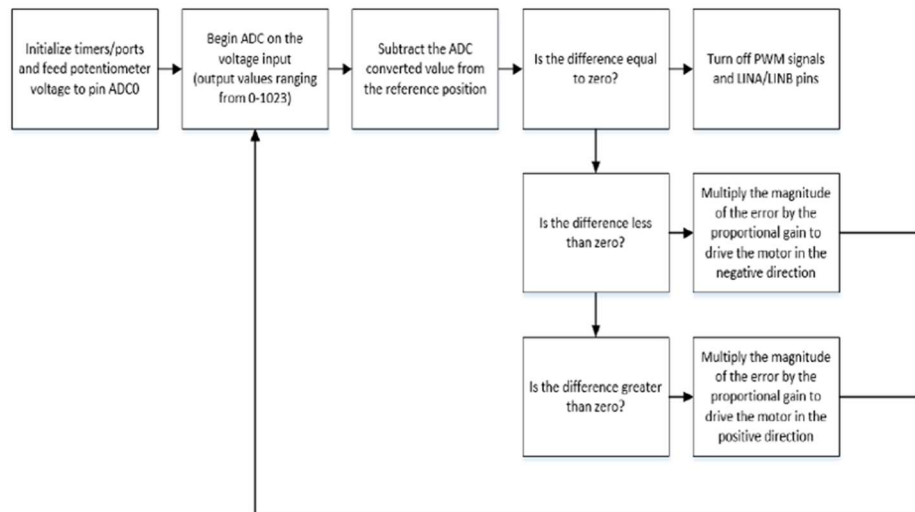


Figure 22-2: Code Flow Diagram for Proportional Controller

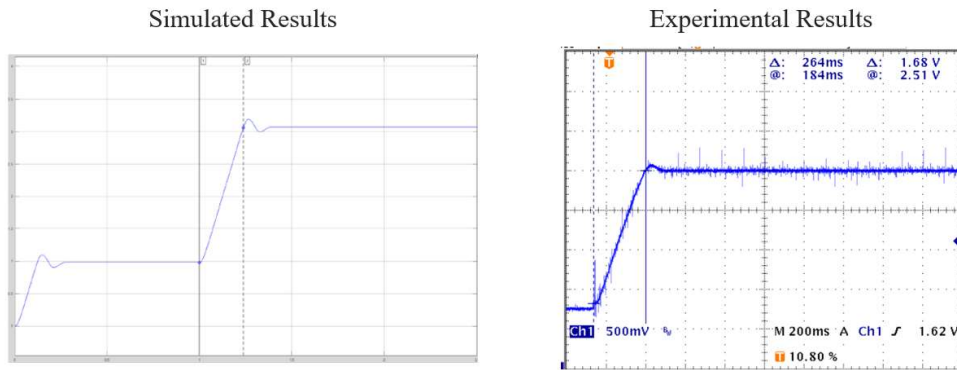


Figure 23-1: Proportional Gain = 5

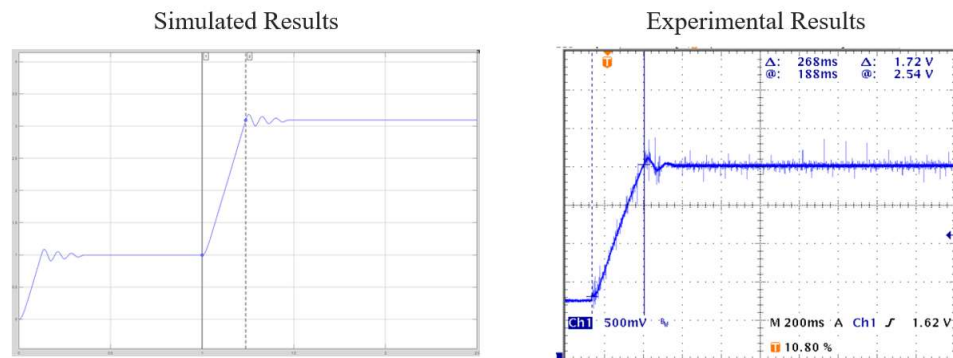


Figure 23-2: Proportional Gain = 10

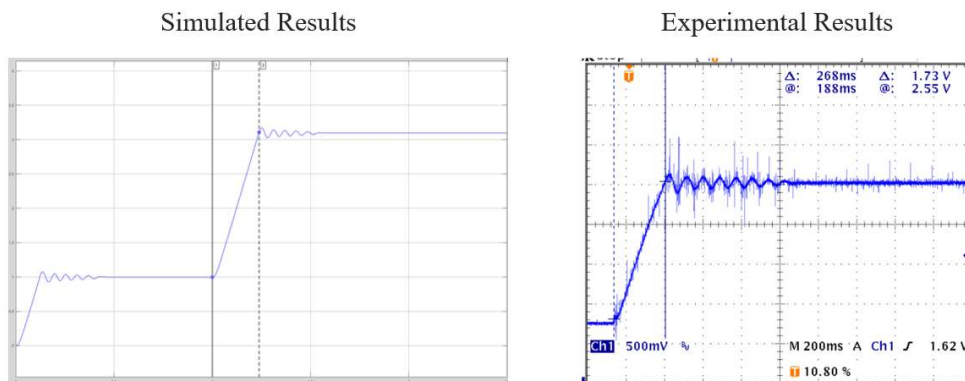


Figure 23-3: Proportional Gain = 15

The microcontroller program for the proportional controller was the same as for the bang-bang controller except that the error between the desired position and the actual platform position was scaled by the proportional gain. The software used for the generation of H-bridge signals was identical to the bang-bang controller, including the 93% limit placed on the duty cycle of the PWM signal to permit time between switching cycles for the bootstrap capacitors associated with the high-side drivers to recharge adequately.

```

int16_t ER = (ref - adc_average);
//int16_t low_ER = ER & 0xFF;
//int16_t high_ER = (ER>>8) & 0xFF;
//PORTA = low_ER;
if(ER == 0)
{
    TCCR0 = 0x00;
    TCCR2 = 0x00;
    //PORTA = 0xFF;
}
else if(ER < 0)
{
    //PORTA = 0x00;
    TCCR2 = 0x00; //TCCR2=0b01101011;
    TCCR0 = 0b01101100; //TCCR2=0b01101011; negative direction
    Vdc = ER*kp;
    Vdc = abs(Vdc);
    if(Vdc > 230)
    {
        OCR0 = 230;
    }
    else
    {
        OCR0 = Vdc;
    }
    PORTE = 0b00000001;
}
else
{
    //PORTA = 0x00;
    TCCR0 = 0x00; //TCCR0=0b01101100;
    TCCR2 = 0b01101011; //positive direction
    Vdc = ER*kp;
    Vdc = abs(Vdc);
    if(Vdc > 230)
    {
        OCR2 = 230;
    }
    else
    {
        OCR2 = Vdc;
    }
    PORTE = 0b00000010;
}
}
}

```

Figure 24-1: Proportional Controller Code with Duty Cycle Scaling and Position Control

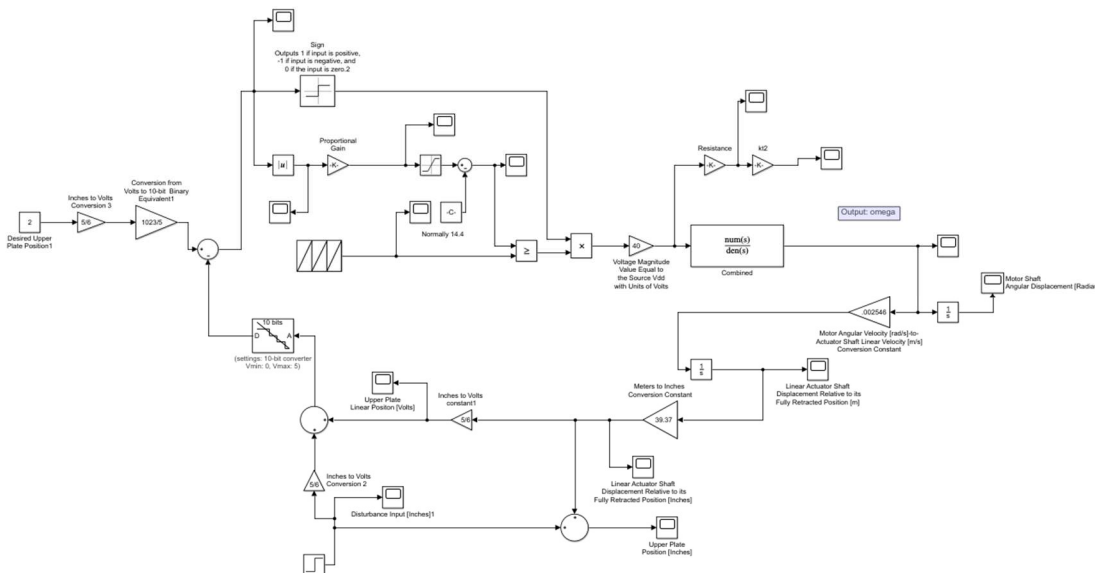


Figure 24-2: Final Proportional Controller Simulink Model

K. Keypad and LCD:

To provide user input to permit selecting the desired upper platform position, the team utilized the keypad and LCD screen available on the Atmega128A microcontroller board. The user can enter position values ranging from 2 to 4 inches with a resolution of one tenth of an inch. Figure 25-1 shows the program flow diagram for the keypad logic.

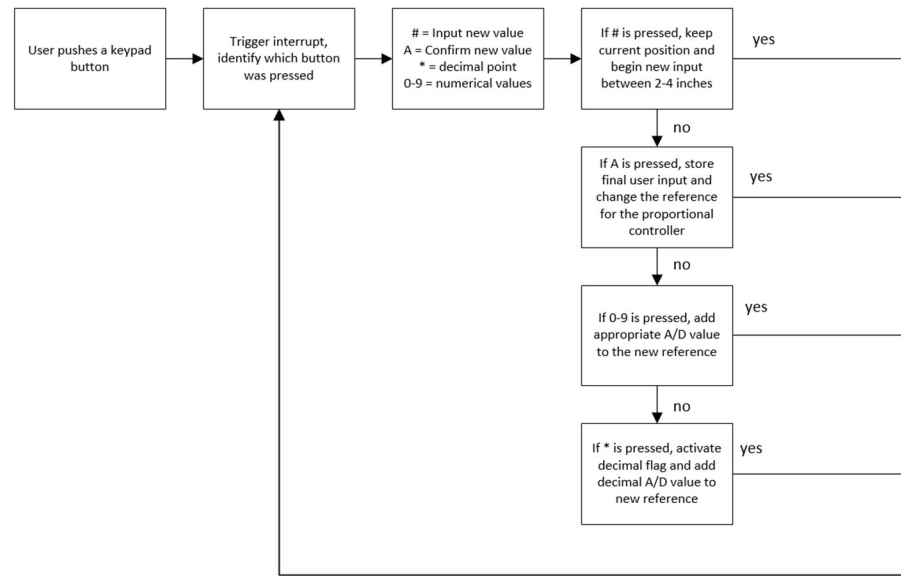


Figure 25-1: Keypad Logic Software Flow Diagram

The initialization and interrupt routines associated with the keypad and LCD are taken from the interfacing lab the team had taken in their junior year. The keys utilized are the numeric values 0-9, A, #, and *. The # key is used to request a new reference position for the upper platform, and clears the LCD screen in preparation for displaying the value for the new position. The numeric keys are used to enter a position between 2 and 4 inches, with the * key being used to represent the decimal point character. As the values are entered on the keypad, they are immediately displayed on the LCD screen for viewing. Pressing the A key will accept the new reference position and signals the microcontroller to modify the proportional controller to move the upper platform to the new position.

When a numerical button is pressed, it modifies a binary value stored in a temporary variable corresponding to the position (in inches) representing the user input. Once A is pressed, the temporary value is set equal to the reference value in the main while loop of the proportional controller.

An improvement suggested for a future team is to use the timer interrupts to ensure that the keypad entry process does not interfere with critical timing associated with updating the current position value obtained from the ADC, the PWM signal duty cycle, or the linear actuator motor direction.

L. Frequency Responses

After implementation of the proportional controller using the approximate model discussed Section I, frequency response plots were obtained from the team's comprehensive Simulink model based on the viscous friction computed using the product $b\omega$. A sinusoidal input voltage with a constant maximum amplitude of 70[V] was applied to the Simulink model over the frequency range of 0.5 to 50[Hz] to obtain data needed to generate the simulated magnitude and phase frequency plots shown in Figures 26-1 and 26-2. In appendix 1-A, there is a MATLAB file with a two-channel Simulink scope that shows the sinusoidal input voltage and angular velocity, ω , used to generate one point on the frequency response plots. The time lag between the maximum values of the input voltage and output motor radian frequency were used to compute the phase shift at each frequency, and the maximum values of the input voltage and output motor radian frequency were used for magnitude ratio calculations. Appendix 4-A contains all of the simulated data that was used to generate Figure 26-1, 26-2, 28-1, and 28-2.

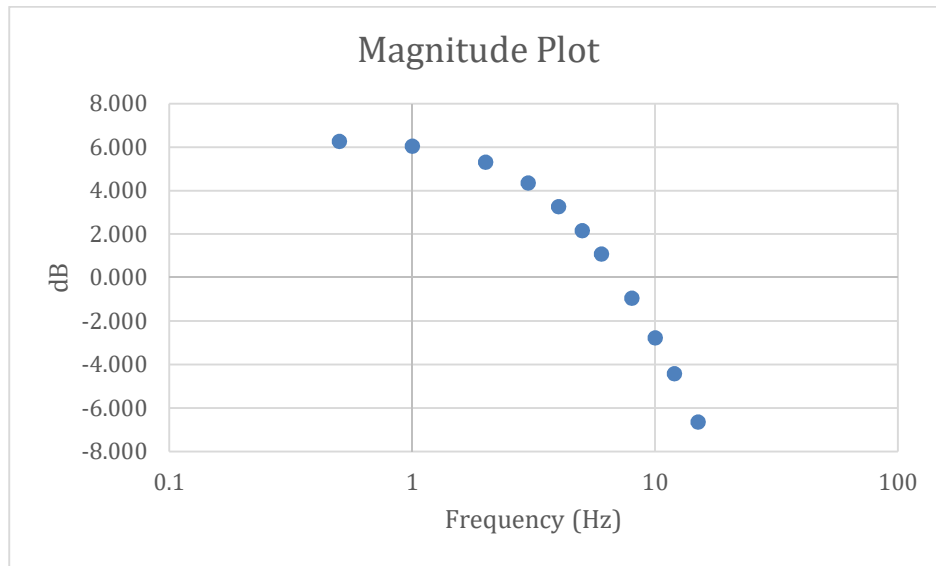


Figure 26-1: Magnitude vs Frequency Plot Obtained from the Comprehensive Linear Actuator Simulink Model Using $b\omega$ to Represent Viscous Friction

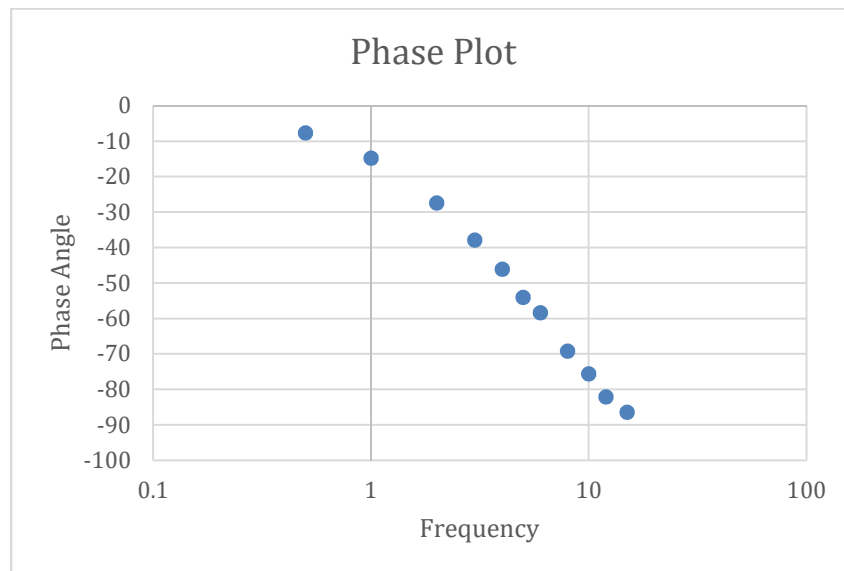


Figure 26-2: Phase Angle vs Frequency Plot Obtained from the Comprehensive Linear Actuator Simulink Model Using $b\omega$ to Represent Viscous Friction

Once Figures 26-1 and 26-2 were generated, the plots were analyzed to determine the 3-dB down frequency for the magnitude plot. The DC Gain, G , associated with the magnitude versus frequency plot is $G = 6.277\text{dB}$, and by subtracting 3 from G , the 3-dB down frequency will occur when the plot reaches a value of 3.277 dB . The 3-dB value then has to be translated into a magnitude by using Equation 26-1.

$$\text{Eq. 26-1: } \text{Phase Angle} = t_L \cdot \frac{360}{f}, \quad t_L = \omega_{max} - V_{s_max}$$

The 3-dB value is then translated to a magnitude by applying Equation 26-2.

$$\text{Eq. 26-2: } 3.277 [\text{dB}] = 20 \cdot \log(M), \quad M = \text{Magnitude}$$

$$M = 10^{3.277/20} \rightarrow M = 1.4583$$

The magnitude is then multiplied by the maximum value of the input voltage, $V_{max} = 70$ [V], to obtain the maximum magnitude of the ω plot, ω_{max} , as shown in Equation 27-1.

$$\text{Eq. 27-1: } \omega_{max} = M \cdot V_{max} = \left(1.4583 \left[\frac{\text{rad/s}}{\text{V}}\right]\right) (70[\text{V}]) = 102.08 \left[\frac{\text{rad}}{\text{s}}\right]$$

After the value for ω_{max} was estimated, more simulations were completed to find the operating frequency that resulted in a motor radian frequency of $\omega_{max} = 102.08$ [rad/s]. The simulations determined that the 3-dB down frequency related to the magnitude plot is approximately 4 [Hz]. The 3-dB down frequency of approximately 4 [Hz] found from the additional Simulink simulations confirmed the value found directly from the plots of magnitude and phase shift versus frequency shown in Figures 26-1 and 26-2. Note that the 3-dB down frequency in the magnitude versus frequency plot corresponds to the -45[degree] point on the phase shift versus frequency plot.

The Mechanical System transfer function will follow Equation 27-2. The DC gain that relates to the magnitude plot shown in Figure 25-1 is set equal to the reduced transfer function.

$$\text{Eq. 27-2: } \frac{\omega}{V_{in}} = \frac{K}{s+p}$$

The pole relating to the break frequency must be found, in addition to the gain related to the system. The pole of the system, p , can be found by implementing Equation 27-3, and at DC, the s -term in the denominator goes to zero, and Equation 27-4 shows the calculation of K .

$$\text{Eq. 27-3: } p = 2\pi \cdot f_B \left[\frac{\text{rad}}{\text{s}}\right]$$

$$p = 2\pi \cdot 4 \text{ [Hz]} = 25.1 \text{ [Hz]}$$

$$\text{Eq. 27-4: } K = G_0(s) \cdot p, \text{ where } G_0 \text{ is DC Gain}$$

$$K = G_0(0.5) \cdot 25.1 = 2.06 \cdot 25.1 = 51.77$$

With the k and p found, the resulting transfer function of the Mechanical System is:

$$\frac{51.77}{s + 25.1}$$

Eq. 27-5: Transfer Function of the Mechanical System

The transfer function was implemented in a simplistic Simulink model (see Appendix 1-B) to compare the magnitude plot generated by the transfer function shown in Equation 27-5 with the magnitude plot obtained using the comprehensive linear actuator Simulink model using $b\omega$ to represent viscous friction. The simulation process was used to collect adequate data to generate the magnitude plot shown in Figure 26-1 used for comparison with the comprehensive linear actuator Simulink model.

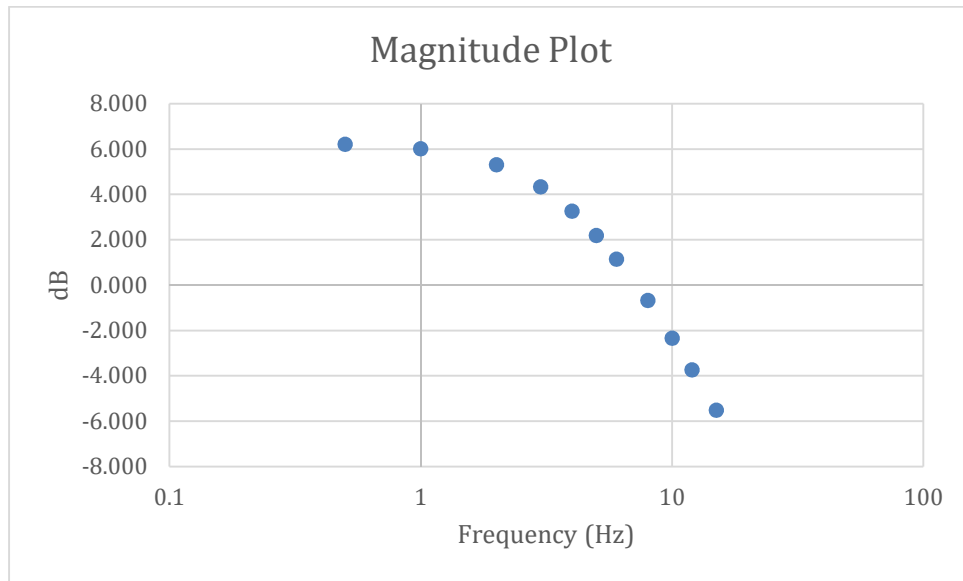


Figure 28-1: Magnitude vs Frequency Plot for the Equivalent Transfer Function Representing the Mechanical Portion of the Linear Actuator System

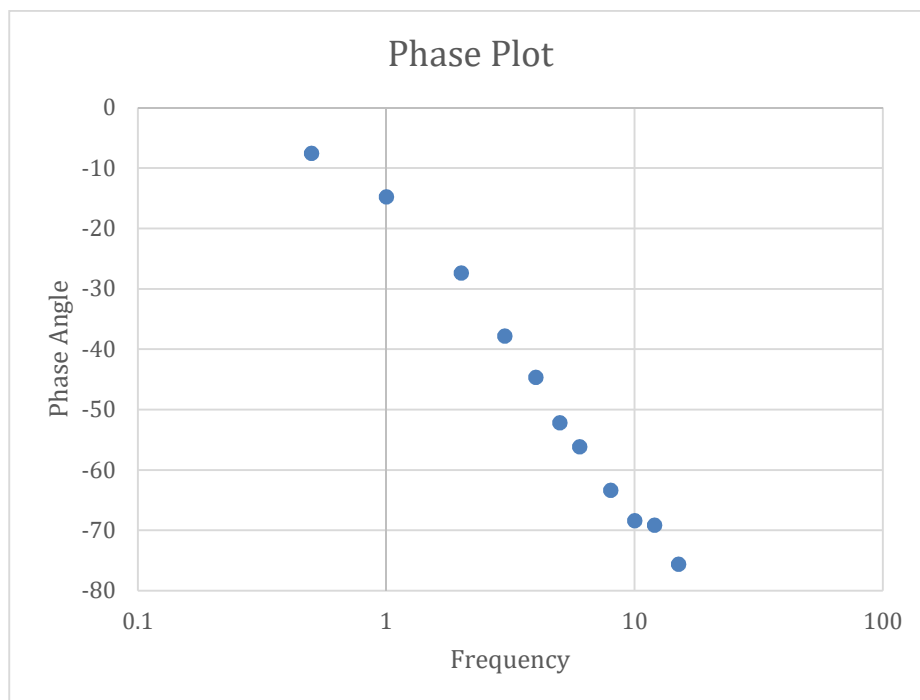


Figure 28-2: Phase Angle vs Frequency Plot for the Equivalent Transfer Function Representing the Mechanical Portion of the Linear Actuator System

Comparison of the magnitude versus frequency plots shown in Figures 26-1 and 28-1 clearly demonstrates that the estimated equivalent transfer function represented by Equation 27-5 accurately represents the comprehensive linear actuator Simulink model using $b\omega$ to represent viscous friction over the expected frequency range of system operation.

VII. Appendices

All files mentioned in the appendices are provided in the Active Suspension System 2019 flash drive.

Appendix 1: Simulink Models

- A. Frequency_Plot_April_19.slx
- B. Frequency_Plot_Final_May_6_New_TF_Theoretical.slx
- C. Gold_Standard_Step_Input_Final_May_6.slx
- D. Linear_Actuator_ver22_Digital_Controller_with_Idiff.slx (Proportional Controller Model)

Appendix 2: MATLAB Code

- A. Ver_18.m

Appendix 3: Embedded C Code

- A. Bang-Bang Controller: "H-Bridge_Switching_adc_v2.zip"
- B. Proportional Controller: "Proportional_Controller_Code.zip"
- C. **Tc and b calculations**

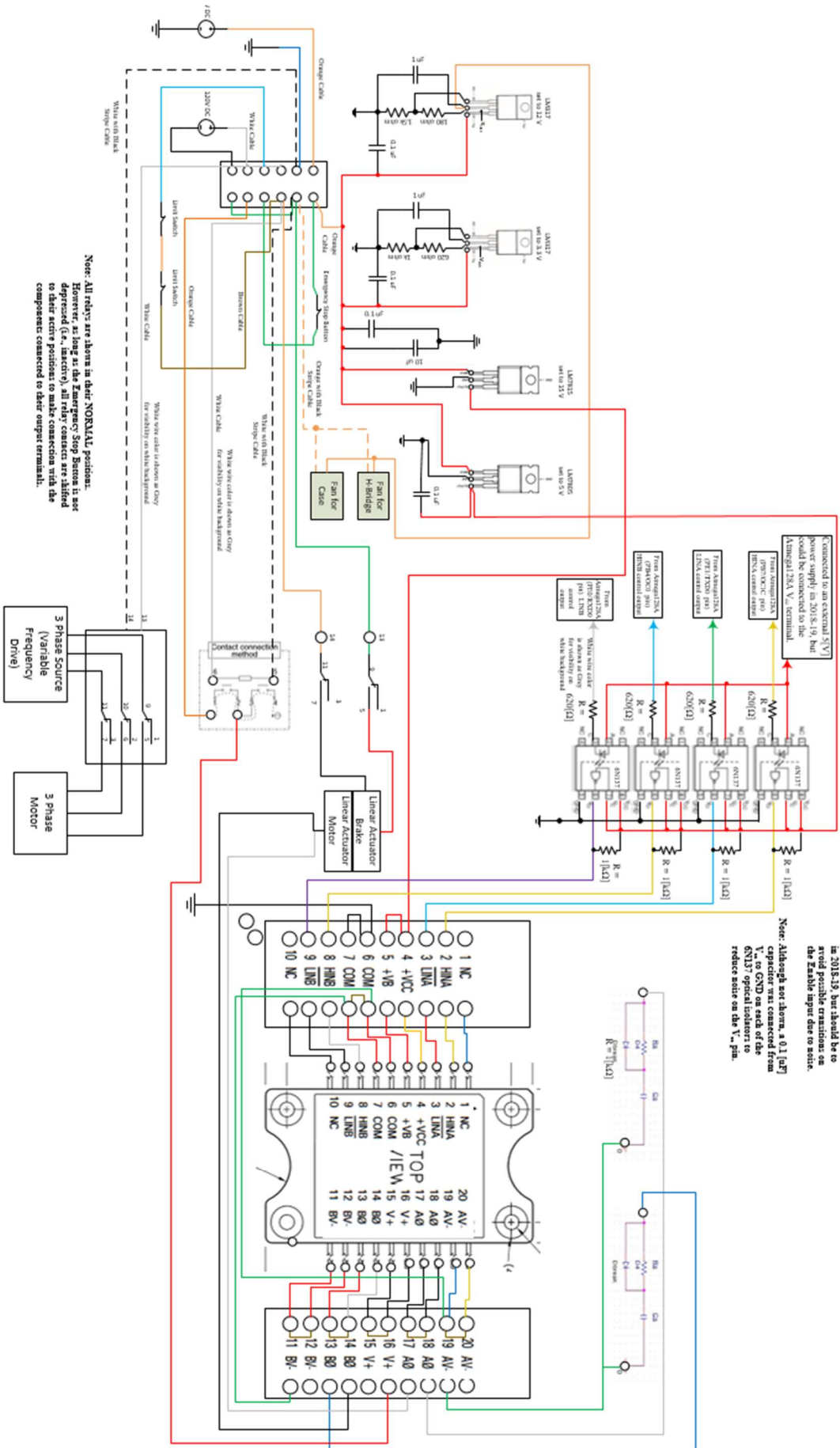
Appendix 4: Spreadsheets

- A. Frequency Response Final May 9
- B. Controller Calculations

Appendix 5: Part List

Part	Description	Quantity	Cost [\$]	Supplier	Acquired
Atmega128A Dev Kit	Microcontroller and Development Board	1	25.99	Waveshare	Y
Keypad	Keypad	1	7.49	Vetco	Y
LCD (4D44780)	LCD Display	1	~\$20-30	Vetco	Y
MSK 4227	H-bridge	1	Discontinued	MSK	Y
IDC Electric Cylinder EC2H	Linear Actuator and Brake	1	~540.00	Amazon	Y
AVR Dragon	Atmega128 Programmer	1	51.61	Mouser	Y
6N137	Optical Isolator	4	1.79	Mouser	Y
Maurey Linear Motion Sensor P1613	Position Sensor	1	299.99	Process Industrial Surplus Corp	Y
Maxi-Torq 4z394	3-Phase Motor	1	543.79	Electric Motor Warehouse	Y
VPLE-212	Camshaft	1	43.67	Amazon	Y
ADXL335	Accelerometer	1	6.62	Digikey	Y
51-256.025	Emergency Stop	1	22.67	Newark	Y
HEV2AN-P-DC24V	Power Relay	1	99.31	Newark	Y
MY4N-D2-DC24	4 Pole Relay	2	20.84	Digikey	Y
NBF-32016	Enclosure	1	22.8	Amazon	Y
LM317	Voltage Regulator	2	0.78	Digikey	Y
7805	Voltage Regulator	1	0.52	Digikey	Y
7815	Voltage Regulator	1	0.5	Digikey	Y
EE80251S2-000U-999	Cooling Fan	1	3.42	Digikey	Y
PS21A79	Replacement H-Bridge	2	73.47	Digikey	Y
Kw11-2	Limit Switch	2	3.95	Amazon	Y

Appendix 6: Schematic of the Apparatus



Note: All relays are shown in their **NORMAL** position. However, as long as the Emergency Stop Button is not depressed (i.e., inactive), all relay contacts are added to their active positions to make connection with the capacitors connected to their output terminals.

Note: V+ was not connected to V- on the 6N137 optical isolator in 2015-19, but should be to avoid possible transients on the Enable input due to static.

Note: Although not shown, a 0.1 [μF] capacitor was connected from V+ to GND on each of the 6N137 optical isolators to reduce noise on the V+ pin.

VIII. References

- [1] A. Serreurier, J. Rose, C. Ramseyer, R. Vassey (2017): <http://ee.bradley.edu/projects/proj2017/actss>
- [2] Atmel, “8’bit Atmel Microcontroller with 128Kbytes In-System Programmable Flash,” ATmega128/L Datasheet, 2011
- [3] Avago, “2.5 Amp Output Current IGBT Gate Drive Optocoupler,” HCPL-3120/J312 datasheet, March 21, 2016
- [4] G. Franklin, D. Powell, and A. Emami-Naeini, *Feedback Control of Dynamic Systems*, Seventh. Pearson, 2015.
- [5] Industrial Devices Corp., “Electric Cylinder Overview,” EC2-H Series Datasheet
- [6] Maurey, “Linear Motion Potentiometers,” P1613 Datasheet
- [7] M. S. Kennedy Corp., “200 Volt 20 Amp MOSFET H-Bridge With Gate Drive,” MSK 4227 Datasheet, November 2004
- [8] Omron, “Miniature Power Relays,” MY4N-D2 Datasheet
- [9] STMicrocontrollers, “N-Channel 250V – 22A Power MOSFET,” STP22NS25Z Datasheet
- [10] Texas Instruments, “LM317 3-Terminal Adjustable Regulator,” LM317 Datasheet